Optimal Design of Microarray Immunoassays to Compensate for Kinetic Limitations

THEORY AND EXPERIMENT*⑤

Wlad Kusnezow‡§, Yana V. Syagailo‡, Sven Rüffer‡, Nina Baudenstiel¶, Christoph Gauer∥, Jörg D. Hoheisel‡, David Wild**, and Igor Goychuk‡‡

In this report we examine the limitations of existing microarray immunoassays and investigate how best to optimize them using theoretical and experimental approaches. Derived from DNA technology, microarray immunoassays present a major technological challenge with much greater physicochemical complexity. A key physicochemical limitation of the current generation of microarray immunoassays is a strong dependence of antibody microspot kinetics on the mass flux to the spot as was reported by us previously. In this report we analyze, theoretically and experimentally, the effects of microarray design parameters (incubation vessel geometry, incubation time, stirring, spot size, antibody-binding site density, etc.) on microspot reaction kinetics and sensitivity. Using a two-compartment model, the quantitative descriptors of the microspot reaction were determined for different incubation and microarray design conditions. This analysis revealed profound mass transport limitations in the observed kinetics, which may be slowed down as much as hundreds of times compared with the solution kinetics. The data obtained were considered with relevance to microspot assay diffusional and adsorptive processes, enabling us to validate some of the underlying principles of the antibody microspot reaction mechanism and provide guidelines for optimal microspot immunoassay design. For an assay optimized to maximize the reaction velocity on a spot, we demonstrate sensitivities in the aM and low fM ranges for a system containing a representative sample of antigen-antibody pairs. In addition, a separate panel of low abundance cytokines in blood plasma was detected with remarkably high signal-to-noise ratios. *Molecular & Cellular Proteomics 5:1681–1696, 2006.*

Microarray immunoassays are gaining in importance as an analytical platform for the high throuput detection of proteins in biological fluids (1–3). In the last few years, this technology has progressed greatly with a multitude of new signal generation and detection techniques (3), surface chemistries (4, 5), appropriate recombinant antibody technology (6), and diverse assay formats (2, 5, 7). These can be roughly grouped into antibody, antigen, and reverse phase microarrays as well as multispotting techniques. Nevertheless the applicability of current antibody microarrays for profiling complex biological specimens, which was one of the main tasks that originally motivated the overall development of this technology, is still restricted at the moment. If simple detection strategies are used, such as protein labeling with dyes or haptens, the best detection thresholds achieved tend to be in the nM to mid-pM range (2, 3, 8). Powerful signal-generating systems such as rolling circle amplification (9) or detection by resonance light-scattering colloidal gold particles (10) need to be applied to improve the limit of detection (LOD)[1] and to attain the low fM range analyzing complex biological samples. Successful commercial examples include the Clontech antibody microarray system containing $\sim$380 well characterized antibodies (11) and Zeptosens, protein microarrays enabling detection to 10 pg/ml analyte in serum (12).

However, this situation is inconsistent with the performance predicted by *ambient analyte theory* (13, 14). The ready availability of standard scanner resolutions of 0.1 and less Cy molecules/μm^2, antibodies with a picomolar affinity (10^{-9}–10^{-11} M), and typical density of binding sites in the range of $10^5/\mu m^2$ should ideally allow achievement of attomolar sensitivity even with simple detection approaches. Nevertheless to the best of our knowledge such a high sensitivity has not been demonstrated thus far without using expensive amplification techniques.

In addition to some known reasons such as low stability of antibody molecules, strong background signal due to inevitable protein adsorption on all kinds of surfaces, or even insufficient sensitivity of the detection approach itself, we have

---

[1] The abbreviations used are: LOD, limit of detection; GPTS, (3-glycidoxypropyl)trimethoxysilane; IFNG, interferon-γ; IL, interleukin; KLH, keyhole limpet hemocyanin; TCM, two-compartment model; TG, thyroglobulin; anti-IFNG, monoclonal anti-human interferon-γ antibody; anti-KLH, affinity-isolated anti-hemocyanin antibody; anti-TG, monoclonal anti-thyroglobulin antibody; NHS, *N*-hydroxysuccinimide; PEG, polyethylene glycol.

demonstrated recently a strong domination of the mass transport constraints in the reaction kinetics on examples of a typical antibody microspot assay (15–17). Due to a small binding area, the microspot kinetics depends intrinsically on the analyte concentration. Therefore, even if ideal mass transport-independent incubation conditions could be achieved, the reaction on a microspot may still require many hours, or even tens of hours, to reach the thermodynamic equilibrium at relatively low analyte concentrations (L_0), *i.e.* at $L_0 \ll K_d$ where K_d is the binding affinity constant in M. In contrast to this, the reaction may be accomplished relatively fast at $L_0 \gg K_d$ (few minutes or seconds). To enable analysis of the mass transport dependence of binding reactions on microspots, a mathematical tool was developed in our previous study (15). This tool is based on the so-called two-compartment model (TCM), which is widely used for interaction studies using the Biacore instruments (18–20). TCM dissects the mass transport-dependent binding into two steps: (i) transport of the analyte from the bulk compartment to the reaction area (reaction compartment) and (ii) the subsequent binding process. Using this model, the overall reaction rate in the antibody microspots was found to be strongly impaired by the mass transport constraints, being capable of prolonging the times required for a solution reaction by many orders of magnitude. As a consequence of this, the saturation of signal intensity on a highly affine antibody spot can be achieved only after unrealistically long incubation of tens, hundreds, or even thousands of hours (15, 16).

In contrast to other kinetically relevant effects, *e.g.* related to antibody immobilization (partial denaturation, heterogeneous affinity, steric hindrances for binding, etc.), the strong mass transport limitation of the reaction kinetics seems to be the *primary* physicochemical shortcoming of the current microarray technology. Therefore, the kinetically relevant optimization of microarray parameters aimed to reduce mass transport limitations has to be one of the first and most important considerations in protein microspot assay design. We carried out a kinetic analysis experimentally and using a modified TCM theory to assess some basic design characteristics of a microarray immunoassay such as incubation geometry, spot size, stirring, and binding site density on a spot. Additionally we investigated possible reaction mechanisms underlying the signal development on the antibody microspot and tried to understand the physicochemical nature of several experimental microarray characteristics. Finally by optimizing a conventional assay format with a simple signal generation and detection approach, we achieved aM and low to mid-fM sensitivities for several labeled antigens. Moreover we were able to detect a group of low abundance cytokines in the blood plasma with very high signal-to-noise ratios.

EXPERIMENTAL PROCEDURES

Materials—All chemicals and solvents were purchased from Fluka (Taufkirchen, Germany), Sigma, or SDS (Peypin, France) unless stated otherwise. Untreated slides were purchased from Menzel-Gläser (Braunschweig, Germany). Milk powder, (3-glycidoxypropyl)trimethoxysilane (GPTS), recombinant human interferon-γ (IFNG), monoclonal anti-human interferon-γ antibody (anti-IFNG), keyhole limpet hemocyanin (KLH), and affinity-isolated anti-hemocyanin antibody (anti-KLH) were obtained from Sigma. Thyroglobulin (TG) and monoclonal anti-thyroglobulin antibody (anti-TG) were obtained from HyTest Ltd. (Turku, Finland). For profiling experiments, anti-IL1A, anti-IL1B, anti-IL2, anti-IL4, anti-IL6, anti-IL8, anti-IL10, anti-IL12B, IL15, anti-interferon-α, anti-IFNG, anti-tumor necrosis factor α, anti-transforming growth factor β1, anti-granulocyte-macrophage colony-stimulating factor 2, anti-vascular endothelial growth factor, and anti-fibroblast growth factor 2 were obtained from Acris Antibodies (Hiddenhausen, Germany).

Fabrication of Antibody Arrays—Homemade epoxysilanized slides were manufactured according to the following protocol. Untreated slides were washed with ethanol, then etched overnight by immersion in 10% NaOH, cleaned by sonicating for 15 min, rinsed four times in water, washed twice in ethanol, and derivatized in a 100% GPTS solution at room temperature for 3 h. After silanization, GPTS-treated slides were washed thoroughly with dichloroethane and dried with N_2. The reason for usage of the homemade slides was their lower variability in comparison with the different batches of commercial epoxysilane-coated slides. PBS buffer supplemented with 0.5% trehalose was used as a spotting buffer (21). The antibodies were spotted using an SDDC-2 Micro-Arrayer from Engineering Services Inc. (Toronto, Canada) and SMP15, SMP10, SMP3, and SMP2 pins (TeleChem). The slides were spotted with antibody concentrations of 2 mg/ml in spotting solution if not stated otherwise. It was initially found that different pins produce spots with similar antibody density at this antibody concentration (variation less then 15%; data not shown). The slides for all kinetics experiments were produced so that only one spot could centrally be positioned in every incubation chamber. After spotting the slides were incubated at 4 °C overnight and subsequently blocked for 3 h at room temperature in PBST (PBS with 0.005% Tween 20) supplemented with 4% milk powder. The slides for profiling experiments were spotted with 2 mg/ml antibody in spotting solution. So-called FullArea chips were made by pipetting 30 μl of 150 μg/ml anti-IFNG in spotting buffer on the bottom of a Flexiperm well (Sigma). The Flexiperms were of 3.3-mm well radius and 10-mm height and fixed on the slide surface using double adhesive tape. FullArea chips, where the bottom of the incubation chamber is completely coated by antibodies, were designed to be comparable to the classical ELISA incubation geometry. Incubation and blocking was done as described above.

Antigen Labeling and Incubation—Antigen solution of 1 mg/ml was labeled with the monofunctional NHS ester of Cy3 dye (Amersham Biosciences) as recommended by the manufacturer. Unreacted dye was blocked from further reaction by adding hydroxylamine to a final concentration of 1 M and separated from the labeled proteins by PD-10 columns (Sephadex™ G-25, Amersham Biosciences).

The slides before incubation were first rinsed for a few minutes in PBS and dried by centrifugation to remove an aqueous film on the slide surface that may potentially prolong and modify the reaction kinetics due to the additional diffusion time through this film. Incubation of the microarrays with antigens always occurred in Flexiperms and with the incubation volume of 100 μl (PBS, 4% skim milk, and 0.01% sodium azide) unless stated otherwise. For stirring we usually used the SlideBooster (Advalytix, Brunnthal, Germany), which allows for the simultaneous incubation of up to 12 slides with high agitation efficiency so that *e.g.* up to 48 reactions in Flexiperm format could be processed in parallel. The surface acoustic wave mixing technology of the instrument has no dead volume and allows for the agitation of various reaction geometries (cover glass, microtiter plate well, or

open drop) making it well suited for our investigations (22). The SlideBooster agitation parameters were optimized as indicated previously (15). To test the suitability of the incubation geometry, the following incubation chambers were also used: "slidebox" (chamber size, 15 × 26 × 80 mm), EasySeal with dimensions 16 × 28 × 0.5 mm (ThermoHybaid Ltd., Ashford, UK), and Flexiperm as mentioned above. In contrast to EasySeals and Flexiperms, slideboxes were incubated on a shaker. To avoid potential photobleaching effects especially at long incubation times, all incubation chambers were isolated from light. Incubations were performed under stirring and non-stirring conditions. After the incubation, the slides were rinsed several times with PBST.

For profiling experiments, 1 mg of serum was labeled with 100 μg of biotin-PEG$_4$-NHS (Quanta-Biodesign), and the unreacted reagent was separated from the proteins using Microcon centrifugal units (Millipore, Schwalbach, Germany). After 14 h of incubation with 300 μl/well, the slides were washed two times for 5 min each with PBST and incubated for 30 min with 100 nM ExtrAvidin (Sigma) labeled with Dy647-NHS (Dyomics) in the SlideBooster. Finally the slides were washed five times (5 min each) with PBST.

Scanning and Data Analysis—Fluorescence signals were recorded using a ScanArray5000 unit (Instrument Co.) and analyzed with the GenePix software package (Axon Instruments). The results were stored and managed in an appropriate Microsoft Access database. All data points in this work represent an average of three to six individual measurements obtained.

The development of the microspot intensities over time was analyzed using the analytical solution of two-compartment theory (18–20) as described previously (15),

$$S(t) = S_\infty(1 - W(c \exp(-\Gamma t))/W(c)) \qquad \text{(Eq. 1)}$$

where $S_\infty = S_{max}L_0/(L_0 + K_d)$, S and S_{max} are the maximum steady state, and current and maximally attainable signal intensities, respectively, all three parameters expressed in signal units (SU); $K_d = k_-/k_+$ where k_+ and k_- are the association and dissociation rate constants (M^{-1} s^{-1} and s^{-1}, respectively); L_0 is the initial analyte concentration (M); and t is the time in seconds. $W(x)$ in Equation 1 is the Lambert special function defined as the solution of the equation $W(x)\exp(W(x)) = x$ (23), $c = a\exp(a)$ where $a = k_+L_0S_{max}/(k_-S_{max} + k_m(K_d + L_0))$ is a dimensionless parameter that measures the deviation of the kinetics in Equation 1 from an ideal single exponential kinetics, and $\Gamma = (k_- + k_+L_0)/(1 + k_-S_{max}/k_m(K_d + L_0))$ is the rate of approaching the steady state where k_m is the phenomenological mass transport constant (SU × M^{-1} s^{-1}). Alternatively the experimental data can be fitted to the following equation.

$$\Gamma t = a\frac{S(t)}{S_\infty} - \ln\left(1 - \frac{S(t)}{S_\infty}\right) \qquad \text{(Eq. 2)}$$

Equation 1 can be obtained by inversion of Equation 2 and vice versa. To describe the initial development of signal intensity ($S(t) \ll S_\infty$), one can derive from Equation 2 a simple linear expression,

$$S(t) \approx \frac{S_\infty\Gamma}{1 + a}t = S_{max}v_0t \qquad \text{(Eq. 3)}$$

where v_0 is the initial binding reaction velocity which is given by $1/v_0 = 1/v_{ideal} + 1/v_m$ where $v_{ideal} = k_+L_0$ is the ideal initial binding velocity and $v_m = k_mL_0/S_{max}$ is the mass transport contribution. In the case of mass transport-limited binding ($v_m \ll v_{ideal}$), the initial binding velocity equals approximately the mass transport velocity, $v_0 \approx v_m$.

Under non-stirring conditions, the corresponding binding velocity and mass transport rate can be found from the following approximation. Let us assume a fully absorbing disc ($v_{ideal} \to \infty$) of radius R

homogenously covered by antibodies with the density of binding sites ρ. All of the remaining surface is assumed to be totally reflecting. In the stationary Smoluchowski limit, the rate of absorption by such a disc is known to be $k_S = 4DRL_0$ where D is the bulk diffusion coefficient of the analyte molecules (in cm^2/s). The number of antibodies with antigen bound increases with time as $N(t) = k_St$, and the signal increases accordingly as $S(t) = S_{max}N(t)/N_{max}$ where $N_{max} = \pi R^2\rho$ is the total number of antibodies available. On the other hand, in the considered limit we have $S(t) = S_{max}v_mt$ with $v_m = k_mL_0/S_{max}$. From this it follows that $k_mL_0\pi R^2\rho = S_{max}k_S$ and thus

$$k_m = 4DS_{max}/(\pi\rho R). \qquad \text{(Eq. 4)}$$

Furthermore the overall reaction becomes obviously mass transport-limited when the experimentally estimated Damkoehler number,

$$D_{a\text{-exp}} = \frac{v_{ideal}}{v_m} = \frac{k_+S_{max}}{k_m}, \qquad \text{(Eq. 5)}$$

is large, $D_{a\text{-exp}} \gg 1$. For this particular model with k_m in Equation 4,

$$D_{a\text{-theo}} = \frac{k_+\pi R\rho}{4D} \qquad \text{(Eq. 6)}$$

where $D_{a\text{-theo}}$ is the theoretically determined Damkoehler number. It grows linearly both with the spot radius R and with the antibody density ρ, implying that smaller spots with lower antibody density are preferable to minimize mass transport limitations under the model assumptions.

When the stirring is applied, the situation becomes more complicated. In this case, the mathematical response of the rate of mass transport or the Damkoehler number to stirring intensity, diffusion coefficient, spot radius, and density of binding sites is currently not known. Nevertheless the two-compartment model remains a powerful and insightful tool for kinetic analysis if the rate constant of mass transport is experimentally determined. On the phenomenological grounds, an effective diffusion coefficient can be introduced for all the remaining parameters. The effective diffusion coefficient might then be determined using Equation 4 used merely for its definition. However, to have an experimental definition of the effective diffusion coefficient that does not depend on the two-compartment modeling, we determined it experimentally from the FullArea chip measurements (from non-stationary initial binding kinetics) as described below.

To analyze the data obtained from FullArea chips, an equation from the reaction-diffusion theory by Stenberg and Nygren (24–26) was used.

$$S(t) = \frac{2L_0S_{max}}{\rho}\sqrt{Dt/\pi} \qquad \text{(Eq. 7)}$$

Previously determined affinity parameters for anti-IFNG (15) ($k_+ = 527,000$ M^{-1} s^{-1}, $k_- = 0.000322$ s^{-1}, and $K_d = 611.01$ pM as measured by Biacore) as well as binding site density ($\rho = 10^{-11}$ mol/cm^2) were used for this mathematical analysis. Affinity of anti-TG was also measured using Biacore ($k_+ = 45,520$ M^{-1} s^{-1}, $k_- = 0.000998$ s^{-1}, and $K_d = 21.93$ nM). We observed that in the presence of stirring the initial FullArea chip kinetics was described by a square root dependence (as in Equation 7). For this reason, the experimental definition of the effective diffusion coefficient in the presence of stirring was obtained by applying Equation 7 for the corresponding data analysis.

RESULTS

Impact of Different Incubation Geometries on Signal Development—To find the optimal assay geometry, three different
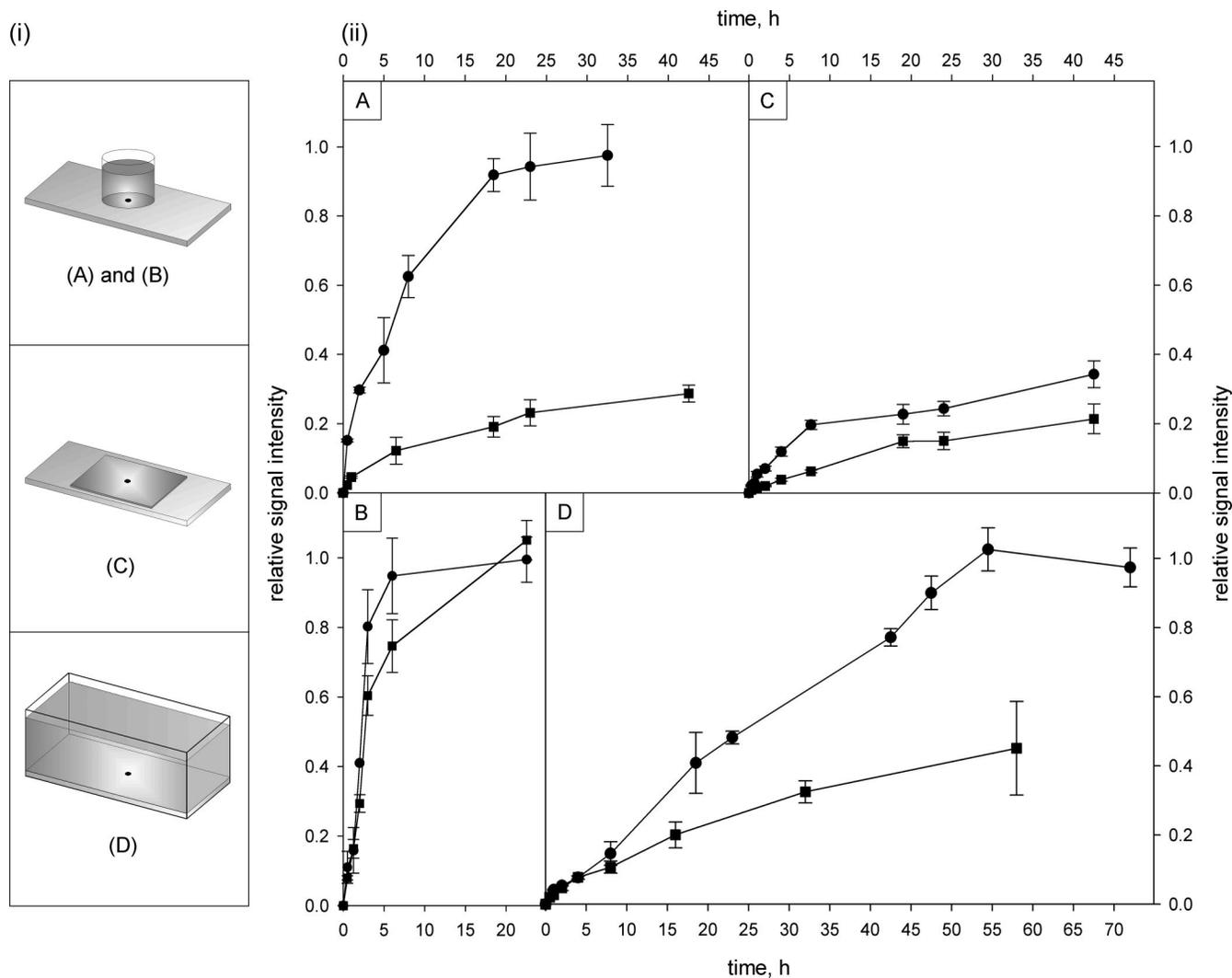

FIG. 1. *i*, different incubation geometries used in the study: well-like incubation chamber (*upper box*), flat geometry EasySeal (*middle box*), and unlimited geometry slidebox (*bottom box*). *Letters* in the boxes indicate the graphs on the *left panel* (*ii*) where the signal development on anti-IFNG spots was measured within the corresponding geometries. 250 μl of 200 pM IFNG solution were incubated in Flexiperm (*ii*, *A*) and EasySeals (*ii*, *C*), and 5 ml of the same solution were incubated in slideboxes (*ii*, *D*). Flexiperm is additionally presented here with 20 nM concentration of antigen (*ii*, *B*). All incubation geometries were tested under stirring (●) and non-stirring (■) conditions.

designs were tested under stirring and non-stirring conditions. The geometry slidebox (15 × 26 × 80 mm) may be considered as an unlimited incubation chamber (Fig. 1*i*). "Flexiperm" has classical well dimensions with a radius of 3.3 mm and height of 10 mm. "EasySeal" is a typical flat incubation geometry for microarrays with dimensions 16 × 28 × 1 mm. To determine the most effective stirring method, the slideboxes were incubated on a shaker at 150 rpm. This condition was found to be the most intense, leading to the highest attainable signals in this system.

Development of signal intensities was observed on anti-IFNG spots printed with SMP3 pins (spot radius, about 90 μm) with a 200 pM concentration of IFNG. Note this analyte concentration is below the K_d value of the IFNG antigen-antibody pair (about 611 pM), and therefore the progression curves

were close to the maximal duration. The well chamber was the best performing system and required stirring for more than 20 h to reach maximum signal intensity (Fig. 1*ii*, *A*). In comparison with this, the incubation using flat EasySeals resulted in up to a 6-fold decrease in signal intensity at the initial time points, whereas only 30–40% of the maximum could be attained after 2 days using this format (Fig. 1*ii*, *C*). Under non-stirring condition, it was impossible to reach the saturation of signal intensity for any of the geometries tested. Also application of the standard glass coverslip usually used for microarray incubations revealed a strong decrease in signal velocity even in comparison with the EasySeals. The data for coverslips are not shown because it was not possible to detect signal at the initial time points, and the weak signal during the incubation was highly variable (see also Ref. 15).
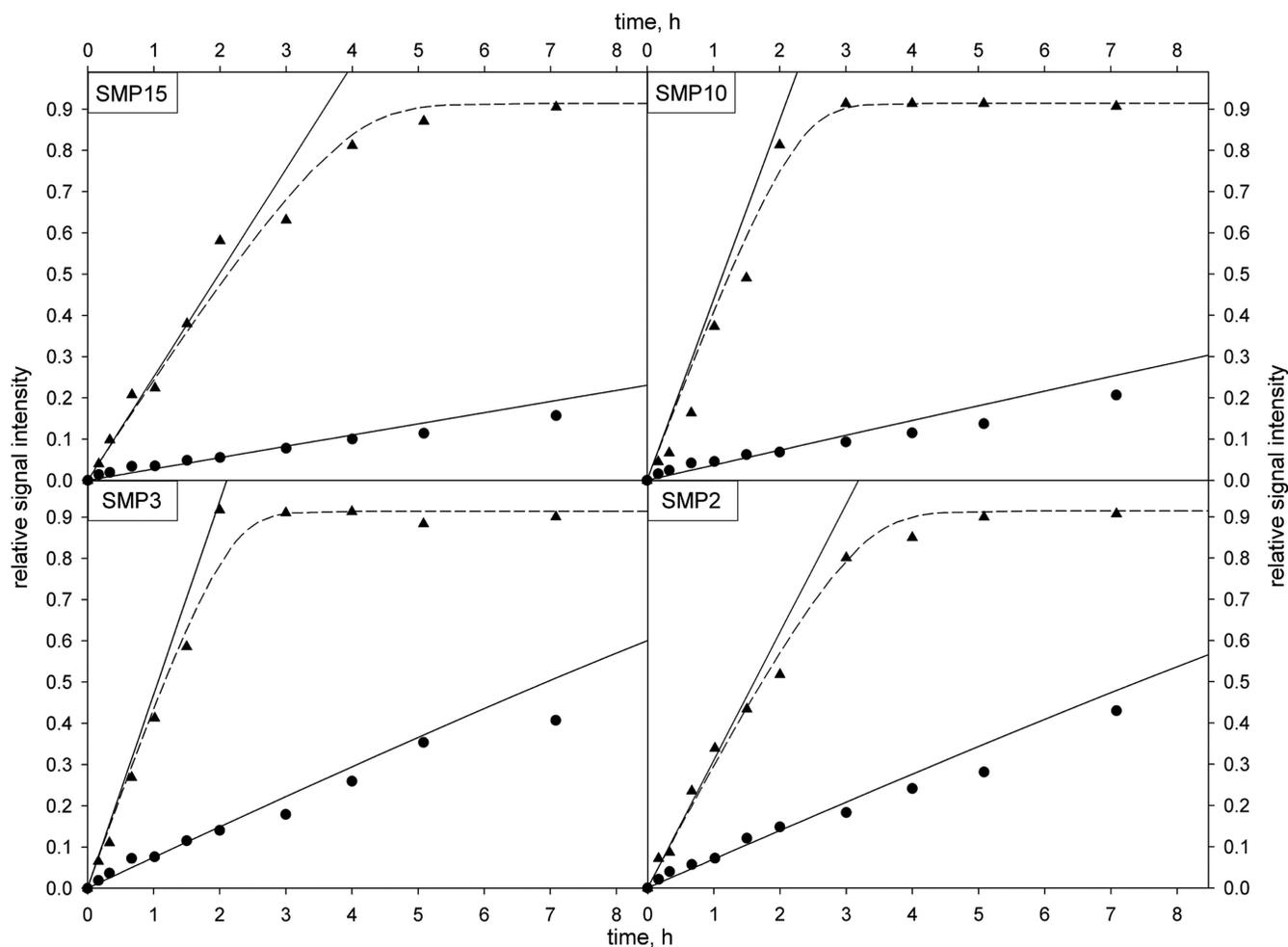
FIG. 2. **Development of the relative signal intensity over time for the anti-IFNG spots of different radius: SMP15 (272-μm radius; *upper left*), SMP10 (190 μm; *upper right*), SMP3 (86 μm; *bottom left*), and SMP2 (45 μm; *bottom right*) under stirring (▲) and non-stirring (●) conditions.** The progression curves were fitted to Equation 1 (- - -) as well as simulated using Equation 3 (—).

The effect of stirring depended on the geometry of incubation chamber varying from practically no significant difference (coverslip and EasySeals) to a 4–5-fold increase with the well.

All geometries were also incubated with 100 times higher (20 nM) and lower antigen concentrations (2 pM). Predictably at 20 nM, the time required for saturation was much shorter, and the differences between the signal intensities developing under stirring and non-stirring conditions were smaller (Fig. 1*ii*, *B*). When incubating the slides at 2 pM antigen, we first detected signal in the most systems after about 10–20 h of incubation (data not shown). Development of signal intensities was also measured with a few other antibodies against IFNG, TG, and KLH, under different incubation conditions. The reaction times described above were often even more prolonged for these antibody-antigen pairs and were less reproducible (see supplemental Fig. S1 for anti-KLH).

*Mass Transport Dependence on Differently Sized Spots—*The observed progression curves (Fig. 1*ii*) indicate a strong dominance of mass transport in the reaction. As follows from several theoretical considerations (13, 25, 27, 28), the velocity of microspot reactions when limited by diffusion (not mass flux due to the stirring) depends on the radius of the spot, increasing as the spot radius decreases, in an inversely proportional relationship (Equation 4). It is important to note that these theories assume a non-adsorptive, completely reflecting surface as well as a steady-state reaction (or k_m = const, constant mass flux over the whole reaction time). In contrast to this, the reaction velocity would be independent of the spot size if the non-steady-state mass flux is dominant. To analyze the character of this reaction, differently sized anti-IFNG spots were incubated under stirring and non-stirring conditions with 5 nM analyte concentration (see Fig. 2 and Table I). The data obtained were fitted to Equation 1 and Equation 3 where S_{max} was set to 1 for all spots to simplify the analysis and interpretation. In these units, the signal intensities obtained experimentally corresponded to the fractional occupancy of binding sites on the spot, and derived k_m values also related to the fractional occupancy.

The agreement between Equation 1 and the experimental data was very good for all incubation times shown (Fig. 2). For

TABLE I
Experimental and theoretical descriptors of IFNG reaction for differently sized microspots (Fig. 2)

The mass transport rate coefficients (k_m/S_{max}) and the factors describing the reaction slowdown due to mass transport ($D_{a\text{-}exp}$) were obtained experimentally using Equations 1–3 and 5. The values $D_{a\text{-}theo}$ and τ_{steady} were calculated from Equations 6 and 11 using the experimental diffusion coefficients obtained by applying Equation 7 to the FullArea chip kinetics and assuming 50,000 binding sites/μm^2 ($8.33 \cdot 10^{-12}$ mol/cm^2) as measured previously (15). Note that the calculated numbers can be considered only as approximations giving a trend rather than absolute values. The calculation of diffusion coefficients according to Equation 7 is susceptible to strong variations as $S(t) \sim \sqrt{Dt}$.

Pin	Spot radius	Mix/no mix	Experimental		Theoretical	
			k_m/S_{max}	$D_{a\text{-}exp}$	$D_{a\text{-}theo}$	τ_{steady}
	μm		$M^{-1}\,s^{-1}$			s
SMP2	45.2 ± 3.2	+	13,255 ± 365	39.8	14	86
		−	3,014 ± 252	174.9	141	174
SMP3	86 ± 7.6	+	20,073 ± 807	26.3	27	37
		−	3,325 ± 277	158.49	270	143
SMP10	190.4 ± 15.9	+	18,658 ± 1516	28.2	60	42
		−	1,561 ± 166	337.6	597	652
SMP15	272.2 ± 20.3	+	10,766 ± 644	49	85	132
		−	1,242 ± 117	424.3	852	1,033

relatively short incubation times (less than 2 h with stirring and 7 h without stirring), an almost linear signal development for all pin sizes was observed, and this initial progression was fitted using Equation 3. Analyzing the results for different pin sizes, it was found that the velocity of signal development ($k_m L_0/S_{max}$) under non-stirring conditions increased as expected with decreasing spot radius. In the rows SMP15, SMP10, and SMP3 (spot radius between 272 and 86 μm), k_m/S_{max} parameter increased nearly 3-fold under non-stirring and 2-fold under stirring conditions (Table I). However, in the case of SMP2 (45 μm), there was no clear dependence of signal velocity on spot radius.

The same experiments were also carried out with the TG antigen-antibody pair, which has a substantially larger analyte (molecular mass of 670 *versus* 17 kDa for IFNG) (Fig. 3) and consequently a 3–4-fold lower diffusion coefficient. The diffusion coefficients can be estimated by the relation $\sqrt[3]{m_1/m_2} = D_2/D_1$ where m is the molecular mass in kDa. The TG antigen/antibody interaction may therefore demonstrate an alternative reaction behavior and is interesting as an example of a microspot reaction with very large molecules. In this case, the signal velocity was independent of the spot radius under non-stirring conditions. Moreover the signal intensity for the large pins developed even faster than for the small pins under stirring conditions. Even under strong stirring conditions, the kinetics for both antigen-antibody pairs still remained substantially mass transport-dependent ($D_{a\text{-}exp} \gg 1$, see also Tables I–III). Moreover the reactions on spots of different sizes demonstrated relatively different susceptibilities to stirring and seem to have an irregular dependence on spot radius for both antigen-antibody pairs (Figs. 2 and 3).

Influence of the Antibody Spotting Concentration on Signal Development—In the Biacore instrument, where the entire surface of the chip is coated with receptor molecules, if the binding site density is reduced there is usually a proportional decrease in the mass transport dependence of the overall reaction rate as would be expected by analogy with Equations

4 and 6. To analyze this parameter in the microspot format, slides were spotted using SMP2 (45 μm) and SMP15 (272 μm) pins with various antibody concentrations in the spotting solution (1000, 250, and 50 μg/ml) and incubated with 20 and 4 nM IFNG or TG for a maximum time of 22 h. Unfortunately this experiment could only be done with stirring because without stirring signal intensity was very low or undetectable (Figs. 4 and 5).

The experimentally determined Damkoehler number ($D_{a\text{-}exp}$, Equation 5) was found not to decrease by the same proportion as the reduction of binding site density as in Equation 6. It decreased only 2–3 times upon a 40-fold decrease in the antibody spotting concentration (Tables II and III). Even at the lowest tested ρ, the microspot reaction remained strongly mass flux-dependent. Also the k_m/S_{max} and/or $S_{\infty\text{-}exp}$ values obtained at 50 μg/ml differed strongly between both tested concentrations of IFNG, whereas, especially in the case of SMP2 spots, $S_{\infty\text{-}exp}$ obtained for 4 nM was nearly 3-fold lower in comparison with 20 nM (both concentrations are well above K_d of antibody), and the progression curves seem to remain in a stationary state, not developing further. The same irregularities were also observed for the case of TG antigen-antibody pairs where they were even more imprinted (Fig. 5, and Table III). Namely based on the affinity parameter of anti-TG as measured by Biacore, the difference between S_∞ values for 20 and 4 nM has to be about 3-fold. Although the expected differences were still obtained at 1 mg/ml on SMP15 and SMP2 spots, spots printed with 50 μg/ml demonstrated much lower, seemingly saturated signal intensities (*e.g.* about 50-fold lower $S_{\infty\text{-}exp}$ at 4 nM as compared with 20 nM on SMP2 spots). Also as in the case of anti-IFNG, k_m constants differed strongly at low ρ, whereas the progression curves still seemed to keep their exponential form and steady-state regime. It should be emphasized that these effects appear especially strong on the smallest SMP2 spots for both observed antibodies. In some preliminary experiments, we were unable to obtain signal intensities analyzing 50 μg/ml printed SMP2
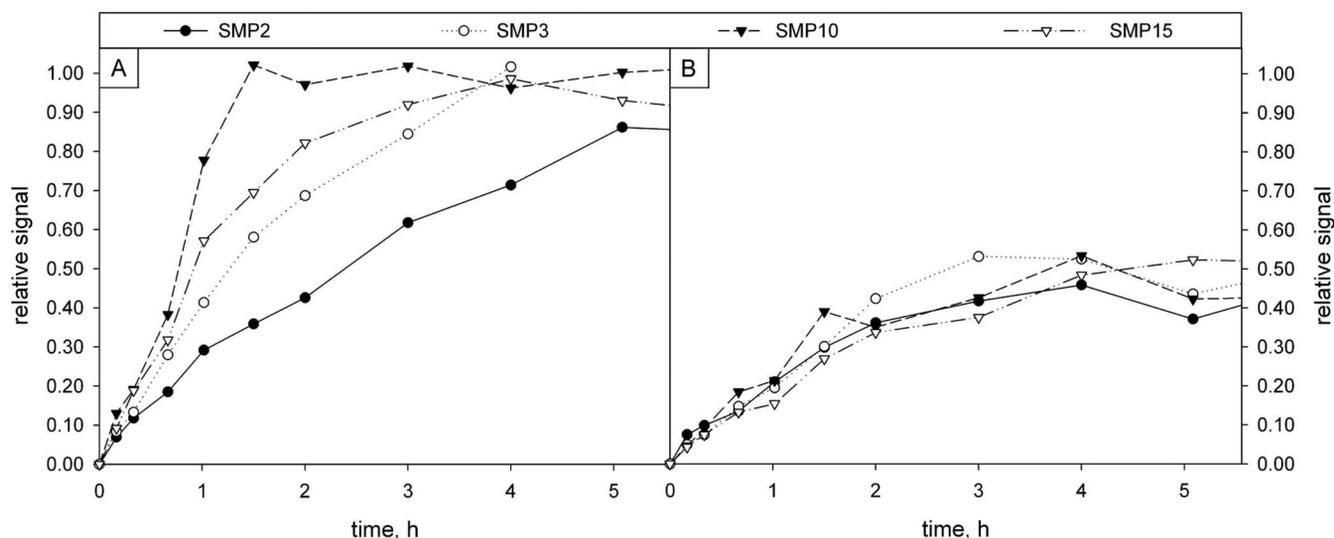
FIG. 3. **Development of the relative signal intensity over time for differently sized anti-TG spots measured with stirring (*A*) and without (*B*).** The TG concentration was 5 nM. The fact that the signal development without stirring is spot size-independent (*B*) serves as an indication of the non-steady-state regime of reaction. Despite the relatively low affine interaction for TG antigen-antibody pair, the significantly lower diffusion coefficient of TG shifts the reaction kinetics into non-steady-state regime (see Equation 11). Non-linear dependence on the spot radius is also observed under stirring conditions (*A*).

TABLE II

Experimental descriptors of IFNG reaction obtained for SMP2 (45-μm) and SMP15 (272-μm) spots with different binding site densities (Fig. 4)

The values k_m/S_{max} were determined by fitting experimental data with Equations 1 and 2, $D_{a\text{-}exp}$ is then obtained using Equation 5, and $S_{\infty\text{-}exp}$ is estimated by comparing the signal intensities reaching saturation with the maximal signal attained at 2 mg/ml spotting concentration and 100 nM analyte concentration, which was taken as the reference value $S_{\infty\text{-}exp} = 1$. To estimate the impact of antibody spotting concentration, $S_{\infty\text{-}exp}$ values can be directly compared with the maximal attainable signal intensities at the corresponding analyte concentrations (20 nM, −0.97; 4 nM, −0.87). The $S_{\infty\text{-}exp}$ value in parentheses deviates strongly from one expected from the binding affinity. The values with ~ could be estimated only approximately.

	Analyte conc					
Spotting conc	20 nM			4 nM		
	$S_{\infty\text{-}exp}$	k_m/S_{max}	$D_{a\text{-}exp}$	$S_{\infty\text{-}exp}$	k_m/S_{max}	$D_{a\text{-}exp}$
μg/ml	SU	$_M{}^{-1} s^{-1}$		SU	$_M{}^{-1} s^{-1}$	
SMP15						
1,000	0.728	13,960	37.8	0.644	14,910	35.3
250	0.292	16,770	31.4	0.287	17,020	30.9
50	0.1237	22,350	23.6	0.100	32,540	16.2
SMP2						
1,000	0.728	18,940	27.8	0.6683	16,750	31.5
250	0.131	17,100	30.8	0.107	30,510	14.8
50	0.030	~30,000	~18	(0.014)	~50,000	~10

spots with subnanomolar (800 and 160 pM) IFNG concentrations (data not shown). To prove whether this quasistationary state can be overcome by a much longer incubation time, the slides printed with SPM3 and different antibody concentrations from 1000 to 125 μg/ml were incubated over 30 h with the dilutions of the corresponding antigens from 100 nM to 2 pM (see supplemental Fig. S2). The signal intensities obtained were normalized against the signal obtained at the 100 nM concentration. Even at 125 μg/ml, both antibodies, anti-IFNG and anti-TG, still demonstrated a strong, 2–4-fold decrease of the relative signal intensities at relatively low L_0 so that the dose-response curves deviated from the results expected from the corresponding K_d values.

Analysis of the Mass Transport Dependence of Classical Well Assays—With the dual goals of estimating the diffusion coefficient of the IFNG molecules in our medium and comparing the kinetics of classical well assays with microspots, the FullArea chips were incubated with 100 μl of 4 nM IFNG for an incubation time of up to 56 h. In the context of our study, the FullArea chip can also be considered as a spot with an infinite radius representing non-steady-state kinetic limit.

Half of the maximum signal intensity was detected in this system after about 30 min of incubation with stirring and after 7 h of incubation without stirring (Fig. 6). The initial part of the progression curve was fitted using Equation 7, which gave the IFNG diffusion coefficient of $1.05 \cdot 10^{-7}$ cm^2/s without stirring

Experimental descriptors of TG reaction obtained for SMP2 and SMP15 spots with different binding site densities (Fig. 5)

The calculation of the k_m/S_{max}, D_{a-exp}, and $S_{\infty-exp}$ values was made in the same manner as in Table II. $S_{\infty-exp}$ values in parentheses deviate strongly from those expected on the basis of the corresponding binding affinity. The values with ~ could be estimated only approximately. Relatively small D_{a-exp} values indicate the irregular character of the spot size dependence of the TG reaction as it can be seen from Supplemental Fig. S2A and Equation 10.

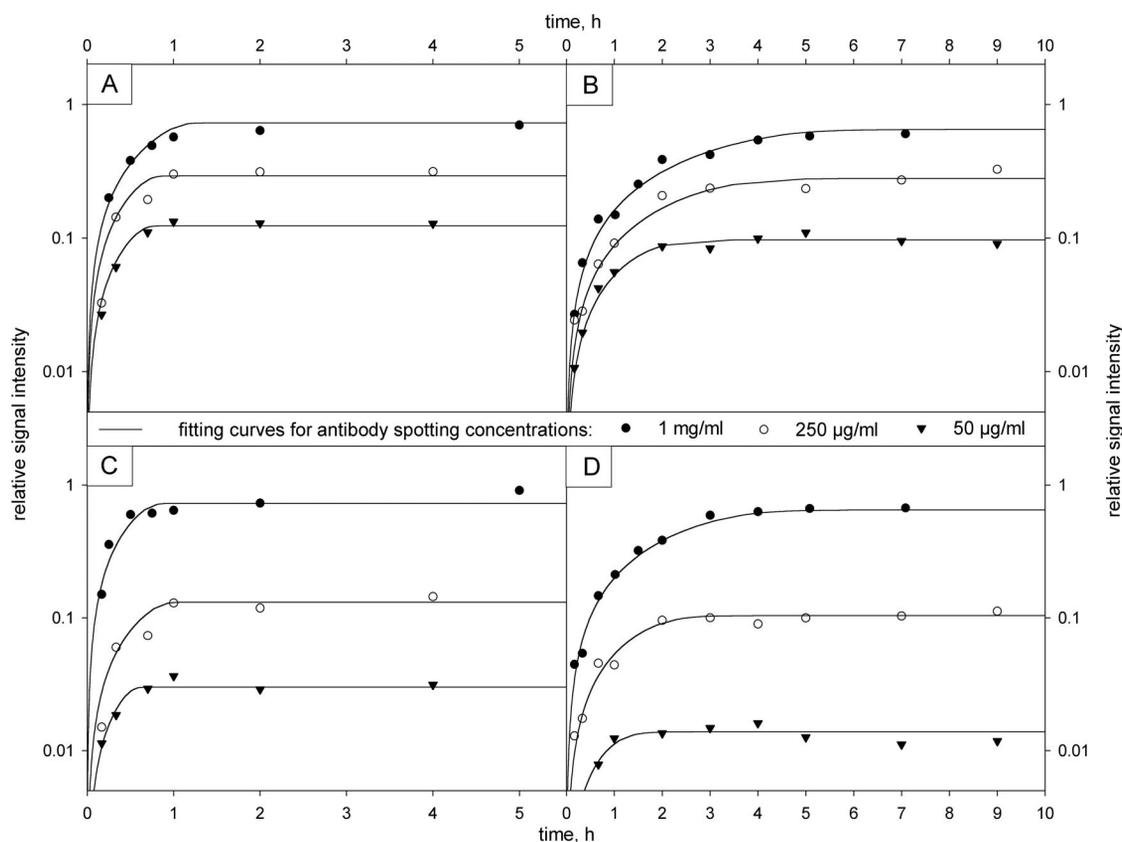| Spotting conc	Analyte conc					
	20 nM			4 nM		
	$S_{\infty-exp}$	k_m/S_{max}	D_{a-exp}	$S_{\infty-exp}$	k_m/S_{max}	D_{a-exp}
$\mu g/ml$	SU	$M^{-1} s^{-1}$		SU	$M^{-1} s^{-1}$	
SMP15						
1,000	0.443	11,800	3.86	0.172	12,300	3.70
250	0.142	22,810	1.99	0.071	17,070	2.67
50	0.031	38,030	1.20	(0.0069)	(~23,000)	(~1.98)
SMP2						
1,000	0.448	15,010	3.03	0.174	5,000	9.10
250	0.105	14,900	3.05	(0.014)	(~10,000)	(~4.55)
50	0.011	22,070	2.06	(0.00024)		

FIG. 4. **Mass transport dependence of IFNG binding on the density of binding sites on the spots.** Signal development on SMP15 (272-μm) (*A* and *B*) and SMP2 (45-μm) (*C* and *D*) spots was observed for different anti-IFNG concentrations in spotting solution: 1 mg/ml (●), 250 $\mu g/ml$ (○), and 50 $\mu g/ml$ (▼). Slides were incubated with 20 nM (*A* and *C*) and 4 nM (*B* and *D*) IFNG concentrations. The signal intensities obtained were normalized upon saturation against S_∞ as calculated from S_{max} - 1 (20 nM - 0.97; 4 nM - 0.87) and subsequently fitted to k_m using Equation 1 (Table II). For graphical presentation, the $S_{\infty-exp}$ values for every progression curve were estimated from the maximal signal intensity obtained at 100 nM with 2 mg/ml printed spots, which was assumed to be the reference value normalized to 1 (Table II).

and the effective diffusion coefficient with stirring of $1.1 \cdot 10^{-6}$ cm²/s. Measuring the diffusion coefficient using fluorescence correlation spectroscopy (Refs. 29 and 30; see also supplemental material) under non-stirring conditions, values in the same range were found (($3.1 \pm 0.89) \cdot 10^{-7}$ cm²/s for IFNG as well as ($1.09 \pm 0.24) \cdot 10^{-7}$ for TG). This difference in the diffusion coefficient determinations may be attributed to the impact of the high milk protein concentration in the incubation solution. The maximum signal intensity reached on the FullArea chips was about 20 times lower than that for the
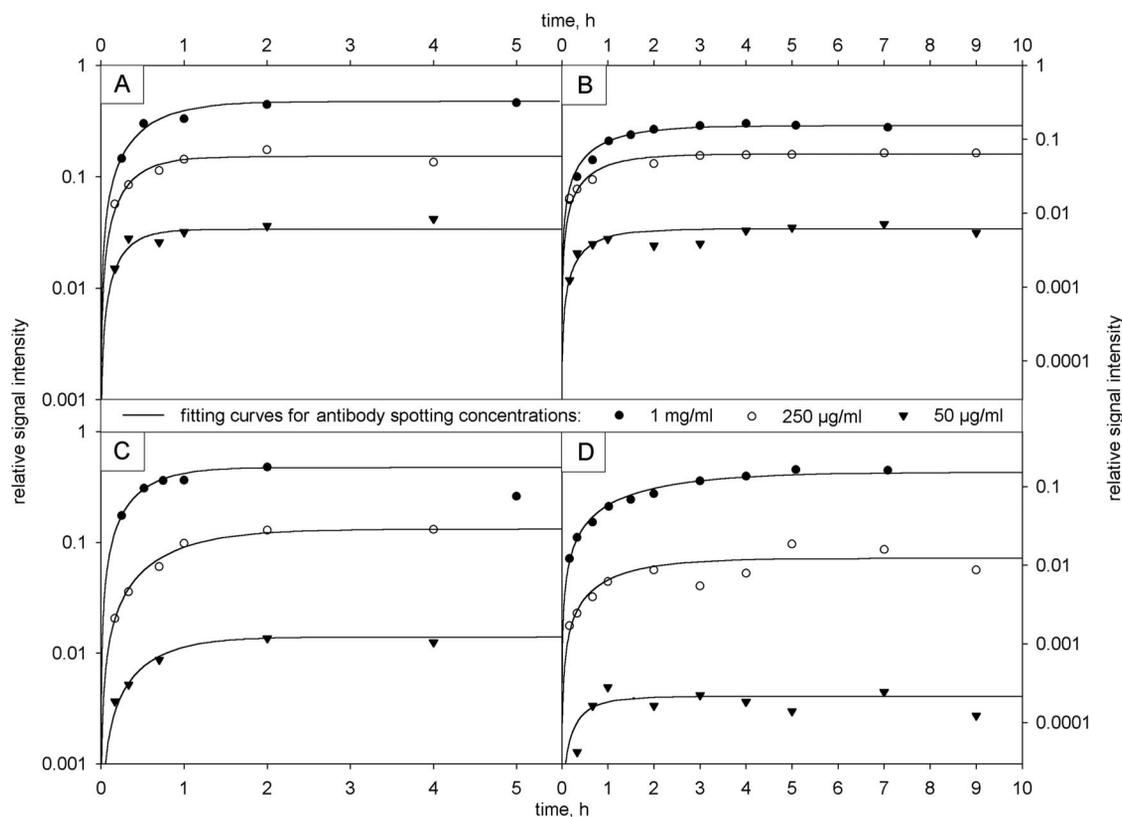
FIG. 5. **Mass transport dependence of TG binding on the density of binding sites on spots.** Signal development on SMP15 (*A* and *B*) and SMP2 (*C* and *D*) spots was observed for different anti-TG concentrations in spotting solution: 1 mg/ml (●), 250 μg/ml (○), and 50 μg/ml (▼). Slides were incubated with 20 nM (*A* and *C*) and 4 nM (*B* and *D*) IFNG concentrations. The data processing was done in the same manner as in Fig. 4.

SMP2 (45 μm) microspot chips incubated in parallel. Incubation of the FullArea chips with 200- and 50-μl volumes resulted in a nearly 2-fold increase and decrease, respectively, in signal intensity obtained upon saturation. Correspondingly a similar slope of progression curve at initial time points was observed for all three volumes (data not shown). This indicates that the FullArea chip detects the whole amount of analyte in the well (not concentration) and that its kinetic behavior corresponds to a classical well assay.

Sensitivity under Optimal Incubation Conditions—As we reported previously, sensitivities in the low fM area could be attained using the simplest direct Cy3 protein labeling (15). However, because signal intensities near to half of the maximal saturation could be ensured by a very long and optimal incubation, the solely relevant limiting factor for further LOD improvement is the sensitivity of the scanner or the quantum yield of the signal detection system. The detection method biotin-PEG$_4$-NHS/Dy647-ExtrAvidin was found to be much more sensitive compared with simple Cy3 labeling.[2] For this reason, it was used in the subsequent sensitivity test and in the protein profiling experiment (Fig. 7).
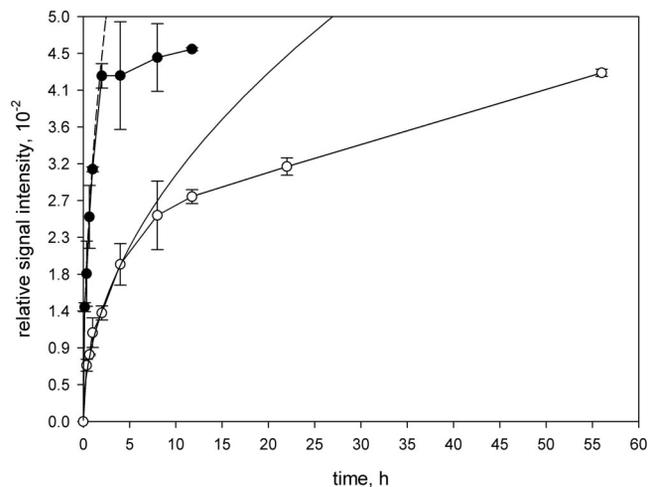

FIG. 6. **Signal development on FullArea chips with stirring (●) and without (○).** Signal intensity on the *y axis* is normalized against the S_{max} obtained on SMP2 (45-μm) microspots. The *lines* (- - - and —) represent simulations of the initial signal development according to Equation 7.

The slides spotted with four different antibodies (anti-IFNG, anti-BSA, anti-TG, and anti-KLH) were incubated with stirring overnight (20 h) using antigen concentration ranges from 1 nM
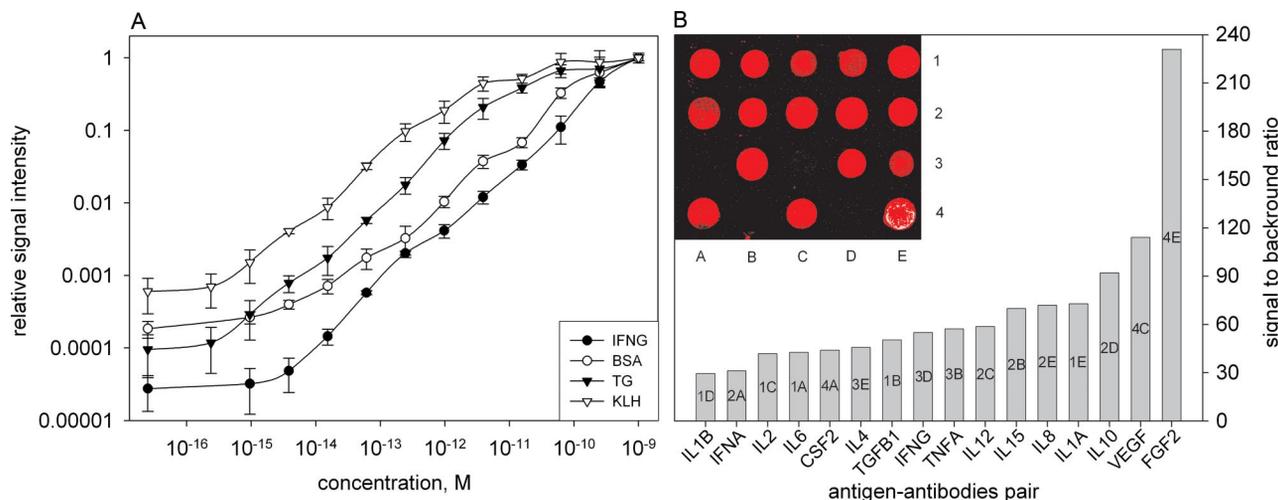
---

[2] W. Kusnezow, V. Banzon, C. Schröder, T. D. Hoheisel, R. Schaal, S. Rüffer, and Y. V. Syagailo, submitted for publication.

FIG. 7. **Performance of the established antibody microarray assay.** *A*, analyte concentration/signal curves attained after 20 h of incubation. The background signal, which was taken for calculation of LODs, is shown in the figure as the smallest concentration. *B*, signal-to-noise ratio obtained in the serum protein profiling experiments. *Positions A3, C3, B4, and D4* contains only spotting buffer. *IFNA*, interferon-α; *FGF2*, fibroblast growth factor 2; *TNFA*, tumor necrosis factor α; *TGFB1*, transforming growth factor β1; *VEGF*, vascular endothelial growth factor; *CSF2*, granulocyte-macrophage colony-stimulating factor 2.

to 60 aM (Fig. 7*A*). The signal intensities obtained were normalized against the maximum signal intensity at 1 nM concentration. With the exception of slides incubated with the lowest two dilutions of antigens, the background signal was generally undetectable in this experiment. LOD was set as 2 standard deviations about the background signal obtained from the slides, which were incubated without analyte (Fig. 7*A*, last concentration points). Anti-TG and anti-KLH were the most sensitive antigen-antibody pairs having LODs between 950 and 240 aM. Two other antibodies, anti-IFNG and anti-BSA, produced signals at least 2-fold higher than the background signal at about 4 fM. All analyzed antibodies demonstrated dynamic ranges of about 5 orders of magnitude. Also in comparison with our previous results, we improved the LODs for KLH and TG antigens by about 10-fold.

To prove the viability of our approach for blood plasma protein profiling, a microarray containing 16 anti-cytokine antibodies was constructed. Whenever possible, the antibodies were chosen in accordance with their binding affinity so that most had K_d values between 1 nM and a few dozen pM. After overnight incubation (14 h) with stirring, we could detect signals from all the spotted antibodies with the signal-to-noise ratios ranging from about 30 up to several hundreds (see Fig. 7*B*). Background was almost undetectable with this scanner adjustment. Because normal concentrations for the investigated cytokines are in the range of a few pg/ml (supplemental Table S1), a low-to-middle femtomolar sensitivity is in fact achieved in our plasma profiling experiments.

DISCUSSION

The primary intent of microarray immunoassays is to replace the classical one-analyte immunoassays, such as ELISA in microtiter well plates, with a sensitive tool aimed for a *multianalyte* analysis of biological samples. On this road, the main obstacle is given by the multiplexity of protein microarray analysis. The assay performance of each analyte-antibody pair in the microarray depends strongly on the protein-specific diffusion coefficients, affinity parameters, and stability as well as their various interface activities. Kinetic effects cause performance to vary across a wide range of analyte concentrations encountered in samples. Also strong mass flux limitations affecting reaction velocity have a much stronger effect than in conventional immunoassays due to the prolonged reaction times in microarray immunoassays. In such a complex multiparametric system, a structured approach is essential for optimization and assay performance measurement.

The magnitude of the mass flux effects on assay kinetics varies enormously. At $L_0 \gg K_d$, the reaction duration depends on L_0 because the time constants for intrinsic ideal reaction and mass transport component are $\tau_{\text{ideal}} \approx 1/(k_+L_0)$ and $\tau_m \approx 1/(k_mL_0)$, respectively. It may therefore be extremely short: a few seconds or minutes (15, 16). On the contrary, more than 4 h of incubation were required at $L_0 \ll K_d$ to obtain the signal saturation for the TG antigen-antibody pair at the highest spotting concentration shown in Table III and Fig. 3*A* ($\tau = \tau_{\text{ideal}} + \tau_m \approx 1/k_- + S_{\text{max}}/k_mK_d$). To estimate the maximal duration of the reaction in the limit of mass transport at $L_0 \ll K_d$, the reaction course can be approximated by the following equation (*cf.* $\tau_{\text{ideal}} \approx 1/k_-$ (15, 16)).

$$S(t) = S_{\infty}(1 - \exp(-t/\tau_m)) \qquad \text{(Eq. 8)}$$

$$\tau_m \approx S_{\text{max}}/k_mK_d \qquad \text{(Eq. 9)}$$

According to Equations 8 and 9, to reach one-half of the maximal signal intensity for the IFNG antigen-antibody pair, about 16 h are required at the best conditions demonstrated

in Table I, whereas saturation would only be attained after more than 60 h. In contrast to this, the same values for SMP15 and SMP10 under non-stirring conditions (Table I) are more than 200 and 900 h, respectively! The corresponding incubation times may have to be prolonged enormously for the assay formats that are not kinetically optimized, for analyte molecules with a low diffusion coefficient, or for antibodies with lower K_d (Equation 9). Because this situation cannot be completely overcome by stirring, the question of crucial importance for those of us developing microarray assays is this: what are the underlying physical principles of antibody microspot kinetics?

In a first order approximation, our system can be modeled in the mass transport-limited environment as a completely absorbing disc placed on a reflecting planar surface. In this situation, one can distinguish between two spot size-dependent reaction regimes: an initial non-steady-state mass transport phase in which the signal develops proportionally to $\sqrt{t}$ and a subsequent steady-state phase where the signal development is proportional to the incubation time t. To match this description with the two-compartment theory, we use a slightly modified equation derived from the diffusion-limited immunoassay theory of Stenberg and Nyngren (24–26). It describes the initial stage of the signal development and reads

$$S(t) = \frac{k_+ L_0 S_{max}}{1 + D_a} t + \frac{2 L_0 D_a^2 S_{max}}{(1 + D_a)^2 \rho} \sqrt{Dt/\pi} \qquad \text{(Eq. 10)}$$

where D_a is the corresponding Damkoehler number. Setting both terms in Equation 10 to be equal to one another, one can extract τ_{steady}.

$$\tau_{steady} = \frac{4 D_a^4 D}{(k_+ \rho)^2 (1 + D_a)^2 \pi} \qquad \text{(Eq. 11)}$$

This is the time after which the first linear term dominates the signal development and the reaction enters the steady-state flux regime where the mass transport to the binding area remains constant ($k_m = $ const). Via the time τ_{steady}, the applicability of our two-compartment approach, which is restricted by the steady-state flux conditions, can be estimated. From the values of the diffusion coefficients and the density of binding sites (10^{-11} mol/cm^2), which both are determined experimentally, it follows that τ_{steady} for the IFNG reaction varies from a few seconds to about 15 min (see Table I) depending on the spot sizes and the incubation conditions. Consequently the analyzed reaction is substantially in the steady-state mass transport regime. Also theoretical D_a values calculated from Equation 6 are in satisfactory agreement with the values derived from our experimental data using Equation 5 (see Table I).

On the other hand, substantially smaller diffusion coefficients of the analyte may result in non-steady-state reaction (similar to the FullArea chip). Note that for $D_a \gg 1$ in Equation 11, τ_{steady} is proportional to R^2/D (assuming that Equation 6 is valid), and it is independent of $k_+\rho$. In this regime, the second term dominates in Equation 10, and the kinetics can be independent of R, k_+, and ρ if $D_a \gg 1$. This is the case for the TG antigen-antibody pair where a dependence of the signal velocity on the spot size under non-stirring conditions was not observed (Fig. 3B). Moreover because $S(t) \sim \sqrt{Dt}$ in such a case, a much stronger mixing strength is required (Fig. 3) to obtain the same amplification factor of the signal velocity as for the steady-state mass transport regime (Fig. 2). Furthermore the TG reaction with stirring (Fig. 3A) is also in line with our theory because the reverse dependence of the v_0 on the spot size may be held if D_a is sufficiently low and $D_a/(1 + D_a) < 1$ according to Equation 10. Summarizing, the kinetic mechanism described by Stenberg and Nyngren (24–26) seems to dominate our experiments demonstrated in Figs. 2 and 3. Moreover the domination of this mechanism can also be assumed for any other antigen/antibody interaction in our system because IFNG and TG antigen-antibody pairs represent two extremes with relatively low and high molecular weight proteins, respectively.

Apart from this simplified picture of the underlying reaction mechanism, nonspecific protein adsorption may significantly influence the binding reactions on surfaces. Proteins that are bound only weakly to the surface (like relatively small IFNG molecules) stay mobile and diffuse on surface until they bind specifically or desorb again (31, 32). It is worth mentioning that an accompanying two-dimensional diffusion is usually considered to be one of the main mass flux mechanisms in the related DNA microarray technology (33). Accounting for the impact of surface diffusion on the microspot kinetics, we can differentiate between two different mass transport pathways: two-dimensional diffusion within the spot (*intraspot surface diffusion*) and diffusion outside the spot (*interspot surface diffusion*).

Upon reaching the area of the spot, the reversibly adsorbed molecules require time to search for the binding sites within the spot in two dimensions, which may result in an additional prolongation of the reaction course. The similar problem of a combined three- and two-dimensional binding reaction was theoretically investigated nearly 2 decades ago in a series of seminal studies (33–36). However, the common feature of these reaction models is that even when the targets occupy as little as 1% of the total surface area, the three-dimensional capture efficiency still dominates the reaction pathway. According to our estimation of antigen-binding site density ($\sim 10^{-11}$ mol/cm^2) and assuming their radius is in the range of 10^{-7} cm, the percentage of surface occupied by targets would be well over 10% at high antibody spotting concentration and close to 1% at the lowest spotting concentration ($S_{\infty\text{-}exp}$ for 50 μg/ml; see Table II). Heterogeneous DNA/DNA interaction, which has been investigated much more thoroughly in this context, reaches maximal hybridization efficiency (*e.g.* in the case of 20-bp oligonucleotides) at a surface

density of immobilized DNA molecules in the range of 10^{-13}–10^{-16} mol/μm^2 (37, 38). Consequently in comparison with the Smoluchowski mass transport limit (Equation 4), the influence of such intraspot two-dimensional diffusion on the reaction kinetics seems to be insignificant at least for sufficiently high antibody spotting concentrations.

Alternatively the binding sites may also be accessible for analyte molecules by interspot surface diffusion pathway. Assuming again that our spot is a completely absorbing disc, one can apply the Adam and Delbrück model (27, 39) of a two-stage diffusion capture to analyze this important issue. The average diffusion time to find the disc directly from the bulk (Smoluchowski average time) is $\tau_s = V/4DR$ where V is the volume of the samples (17). On the other hand, to find the disc in a two-stage mechanism, a ligand in the bulk first has to reach the surface, and assuming that the walls of the incubation chamber are completely reflecting, the average time, $\tau_0 = H^2/3D$ (17), would depend only on the height H of the incubation chamber. Furthermore for an incubation chamber with the radius R_c and if $R_c \gg R$ it takes average time

$$\tau' = \frac{1.1 R_c^2}{D'}\ln(1.2 R_c^2/R^2) \qquad \text{(Eq. 12)}$$

where D' is the two-dimensional diffusion coefficient, to reach the target of radius R via the surface diffusion (27, 34). Because normally $D' < D$, the time τ_0 is typically neglected within the two-stage diffusion mechanism. The same is also valid for our experimental case where τ_0 is much smaller than τ' (at $H \approx 0.3$ cm and $R_c \approx 0.35$ cm). For the absorption rate of the considered disc by a two-stage mechanism one can get the following estimation (27, 34),

$$k_S' = \pi R_c^2 d L_b \exp(E_b/kT)/\tau' = \frac{\pi D' d L_b \exp(E_b/kT)}{1.1\ln(1.2 R_c^2/R^2)} \qquad \text{(Eq. 13)}$$

where d is the width of the boundary layer of surface diffusion that has a characteristic size of several nanometers (the effective radius of action of attractive molecular and electrostatic forces at surface) (40) and E_b is a characteristic energy of nonspecific binding. L_b is the actual bulk concentration of analyte, which is related to L_0 and L_s, concentration of the analyte in the interface area, by the following expression: $L_b = L_0 - L_s \pi R_c^2 d/V$. Ligand concentration is greatly enhanced by the factor of $\exp(E_b/kT)$ in the boundary layer with respect to its bulk concentration so that the initial L_0 may be depleted to a greater or lesser extent due to nonspecific adsorption in the limited incubation geometry. The two-stage diffusion mechanism will provide a dominant route when

$$\kappa = \frac{k_S'}{k_S} = \frac{D'}{D}\frac{\pi d \exp(E_b/kT)}{4.4R \ln(1.2 R_c^2/R^2)} > 1. \qquad \text{(Eq. 14)}$$

The energy of nonspecific binding to the surface (E_b) is typically many times larger than the thermal energy ($kT \approx 2.5$ kJ/mol at room temperature) for protein molecules (40). For example, the energy for adsorption of a 13-residue peptide on colloidal silica was measured to be about 36 kJ/mol (41); binding of relatively small proteins such as lysozyme (14.3 kDa) or RNase A (13.7 kDa) to different chromatographic solid supports was indicated in the range of 13–34 kJ/mol (42–44), and the binding energy of a series of proteins to the aluminum salt ranges from about 30 to 40 kJ/mol (45). Assuming $E_b = 20$ kJ/mol and d corresponds to the molecular size of the IFNG molecules (about 4-nm diameter), the two-stage diffusion mechanism can only be significant in our incubation chamber with $R_c \approx 0.35$ cm for R of only a few μm or even less (the dominating mechanism if $R < (D'/D)10^{-4}$ cm). However, for $E_b > \sim 25$ kJ/mol, this mechanism will be important or even dominant ($> \sim 30$ kJ/mol) for today's typical spots of 50–300-μm radius. From another perspective, the two-stage transport mechanism would quickly gain in dominance (Equation 14) if the spot radius decreases. For example, SMP2 spots (45 μm) would be influenced about 3.5 times more strongly by this mechanism than SMP15 spots (272 μm) in our well geometry. To the best of our knowledge, although such an interspot diffusion mechanism is obvious in hindsight, it has not been considered in connection with the microarray kinetics.

The classical consideration above (Equation 14) is still based on the assumption of an unlimited incubation volume or constant source of the analyte in the system. However, both organic and inorganic surfaces can adsorb a considerable amount of protein from bulk solution (usually μg–ng/cm^2) (46–49). Therefore, nonspecific adsorption, even by a pre-blocked surface, may still partially deplete the initial analyte concentration in a limited volume and separate it into two phases: bulk and interface portions. The reduction of the initial analyte concentration can be described as follows.

$$\frac{L_b}{L_0} = \frac{H}{H + d \exp(E_b/kT)} \qquad \text{(Eq. 15)}$$

For our cylindrical reaction chamber with the height $H = 0.3$ cm ($V = 0.1$ ml), more than one-half of all the analyte would be depleted if $E_b > $ kJ/mol according to Equation 15. The change in the adsorption energy has an exponential effect so that the right terms in Equations 14 and 15 double with every further 0.69 kJ/mol increase. It is noteworthy that the two-stage reaction "pathway" is classically considered as an additional mechanism, leading to the enhancement of the reaction rate due to reduction of dimensionality (27, 33, 34, 36, 45). However, due to the bulk analyte depletion, it may affect even adversely the reaction velocity if D' is relatively low (see Equations 12 and 13).

The kinetic, diffusional aspects are practically absent in the modern protein microarray literature. As a result, they do not receive sufficient attention in the experimental design and development of multiple protein microarray applications. Contrary to this, an optimization of even the simplest design and incubation parameters can have a strong impact on the per-

formance and sensitivity of a microarray assay. In the following, we consider a series of kinetically relevant factors from the viewpoints of the reaction mechanism, as described above, in their importance for the microarray design.

Although intensive **stirring** cannot reduce the mass transport limitations to a negligible level, the understanding of stirring effects on the microspot scale is extremely important in practical context. Highly affine binding reactions measured by Biacore systems also suffer from the mass transport constraints despite a high velocity of the solution pumped through the chip. The reason is that the effective rate constant of the mass transport (to which one can formally relate an effective diffusion coefficient) increases as a cubic root of the pumping velocity only (18, 20, 50); *i.e.* a 1000-fold increase of this velocity leads only to a 10-fold increase of the effective diffusion coefficient as observed in our study (Fig. 6). Unlike the Biacore system, where the receptor molecules cover the whole surface of the chip, the microspot reactions are additionally influenced by the two-stage interspot diffusion mechanism (Equation 14). However, stirring, which improves the access of the analyte from the bulk to the surface, can only weakly affect surface diffusion. Therefore, even if a significant portion of the analyte accumulates near the surface, it can still represent a bottleneck for further increasing the overall reaction rate in microspot assays. Furthermore the spot size- and the binding site density-dependent balance of bulk and surface reaction "pathways" are susceptible to stirring to a different extent. In the case where the intraspot diffusion is irrelevant, the signal velocity on relatively large spots would be amplified proportionally with the increase of the effective diffusion coefficient (see Equation 14 and Table I), whereas with decreasing spot radius only a strongly reduced portion of the analyte diffusing from bulk contributes to the acceleration of the signal development (Equations 12 and 13). As a result, one can obtain under stirring conditions either irregular (Figs. 2 and 3 and Table I) or comparable (51) spot size dependence of the signal velocity.

Given the strong impact of the mass transport and the surface diffusion on the assay kinetics, it is not surprising that the **geometry** of the incubation chamber used (Fig. 1) may have a crucial effect on the reaction mechanism that determines the development of signal velocity in time. Flat incubation geometries may strongly disturb the initial analyte concentration. For example, the binding energy for the classical coverslip ($H = 0.01$ cm) would be $E_b > 25.3$ for 50% analyte depletion as calculated from Equation 15, whereas nearly all of the analyte (>95%) would be adsorbed at $E_b > 32.7$. This would lead to a stronger analyte depletion than in the well geometry and would in turn change the overall reaction mode by moving it toward the two-dimensional interspot diffusion mechanism. Consequently the acceleration of signal velocity by stirring would be hindered in flat incubation chambers (Equation 15 and Fig. 1) because stirring can only slightly influence surface diffusion. Because the coverslip itself plays

the same adsorptive role as the reaction surface, a kinetically improved incubation can be achieved by using a well assay in an open geometry, similar to the one presented here, and by increasing the ratio of the sample volume to contact adsorptive surface.

In terms of the assay "ambience," known to be the most sensitive characteristics of the microarray, the minimally permissible **sample volume** is defined as $V \approx [A]\pi R^2/K_d f_{max}$ for the case of $L_0 \ll K_d$ where $[A]$ is the surface concentration of antibody in mol/cm^2 and f_{max} is the maximal fraction of the analyte molecules bound to the antibodies from the bulk solution (at equilibrium and for $L_0 \ll K_d$). In the case of our IFNG pair with $R = 0.01$ cm and $f_{max} = 0.05$, this volume is ~100 μl. Clearly because saturation cannot be achieved with high affinity antibodies, this volume may be many times lower in accordance with the degree of saturation at $L_0 \ll K_d$ and for relatively short incubation times. However, considering the adsorptive forces in the same manner as in the case of the incubation geometry, the minimal sample volume has to be limited by the degree of nonspecific analyte depletion in the system and, consequently, by the ratio of the sample volume to the adsorptive surface. Otherwise a too low volume would lead automatically to lower reaction rates.

As expected from both the work by Stenberg and Nyngren (24–26) and the modified Adam and Delbrück (27, 39) mechanism described above, a decrease in the **binding site density** ρ would not influence the initial signal velocity. This also means that the parameter k_m/S_{max} in Table II should not change at various ρ, whereas D_a should decrease proportionally with decreasing ρ (Equation 6). In such a situation, the signal intensities obtained upon saturation ($S_{\infty\text{-exp}}$) are also expected to proportionally reflect the differences in ρ. However, our experimental observations indicate that strongly suboptimal **antibody spotting concentrations** can surprisingly result in a kind of stationary regime where a quasi-equilibrium is established on a level that is many times lower than one expected from the thermodynamic equilibrium under the ambient analyte conditions (Figs. 4 and 5 and supplemental Fig. S2). This causes an additional strong decrease of the maximally attainable signal intensity, a phenomenon that seems to intensify with the decreasing analyte concentration and the reduction of spot radius (Tables II and III). A potential indication of the character of this effect might be an increasing role of the intraspot surface diffusion, which might also be a limiting factor in the overall reaction rates at relatively low ρ under stirring conditions. Interestingly enough, the three-dimensional **surface chemistries**, which represent an additional barrier for diffusion, suffer even more strongly from non-optimal spotting concentrations. In a previous study (16), we demonstrated for the same antigen-antibody pairs (IFNG and TG) that a spotting concentration of about 100 μg/ml results (under different incubation conditions) in 10–40-fold lower signal intensity on a Hydrogel surface from PerkinElmer Life Sciences as compared with our homemade epoxysilane

slide. Moreover the signal intensity was at least 100 times lower than one obtained for 2 mg/ml on both surfaces. An additional mechanism of a three-dimensional search of sparsely distributed binding sites within the dense polymer matrix may be responsible for this effect.

The impact of antibody spotting concentration, which can influence the resulting signal intensity (and therefore also sensitivity) tens or even hundreds-fold (see $S_{\infty\text{-exp}}$ in Tables II and III), seems to be largely overlooked in the literature. The antibody spotting concentrations are often not adjusted to the same concentration value. They are usually relatively low and vary strongly in complex antibody microarrays (typically between a few dozen and few hundred μg/ml). The experimental finding of optimal spotting concentrations is usually done under strongly mass transport-limited incubation conditions, and the results do not allow differentiation between different binding site densities at relatively high ρ (for details, see Ref. 16). It is interesting to speculate that the answer to the often asked question, namely, why do the majority of antibodies not work in arrays (52), may have a quite simple answer: the spotting concentration is much too low.

Another factor, which is important for the reaction rates on spots, is the **viscosity** of the incubation buffer. The diffusion coefficient is inversely proportional to it in accordance with the Stokes-Einstein relation (27). Therefore, the viscosity impacts directly the mass transport dependence of the reaction kinetics (see Equation 6). Also **the spotting pattern** of antibodies may affect the signal velocity due to the specific analyte depletion in the surrounding bulk solution as well as in the surface area adjoining the spot. The **concentration of the clinical sample** in the incubation buffer is also a factor of great importance, and it has to be set as high as possible. Even if the signal-to-noise ratio decreases for the abundant proteins due to a faster signal saturation and a higher background signal, the higher reaction rates for scarce proteins would make them more detectable and improve the reproducibility of measurements.

Finally all the parameters discussed above impact the linearity and velocity of signal development. At $L_0 \ll K_d$ (see Equation 3), prolonged **incubation times** can lead to a nearly proportional increase both in signal intensity and sensitivity (compare 20 h with typical 0.5–2 h of incubation). This obvious effect was also observed by Saviranta *et al.* (10), who obtained up to a 15-fold improvement in sensitivity of an antibody microarray after 18 h of incubation as compared with 1 h. Protein microarrays are not much different in this respect to the related DNA microarray technology where incubation over many hours is routine.

Even if the maximal binding capacity is attained during the incubation, a significant proportion of the bound analyte can subsequently get lost because of dissociation during **signal generation and washing stages**. Usually this procedure lasts for 2–3 h in the current systems (9, 10, 53). In a simplest case, the time of the dissociation reaction in the mass trans-

port limit would be the same as in Equation 9 (in reaction limit $\tau_{\text{ideal}} \approx 1/k_-$). Consequently although the number of bound IFNG molecules would scarcely be affected even after 3 h of washing or detection, the bound TG molecules might be almost completely removed during such long time intervals. The extent of dissociation should depend on the spot size, affinity parameters, density of binding sites, and the amount of analyte bound. This issue requires a separate, more detailed investigation.

Our kinetic analysis would be incomplete without a glance at the issues associated with **nonspecific binding**, or **background**. The non-removable background signal results from the irreversible adsorption of high molecular weight proteins, which have a relatively low diffusivity. In contrast to the mainly linear signal development on the spots, the adsorption kinetics on flat surfaces is usually considered to be in a non-steady-state regime where it is directly proportional to $\sqrt{t}$ (similarly to the second term in Equation 10; see also Fig. 6). Consequently stirring cannot accelerate the development of background signal to the same extent as for the signals on spots. Background signal is clearly independent of the spot size, binding site density, and the height of incubation solution at the initial time. Development of background signal would proceed in the flat incubation chambers relatively easily as compared with the specific binding on spots due to shorter diffusion distances. Therefore, the microarray analysis of complex biological samples clearly benefits from the kinetically optimized design. The achievement of femtomolar sensitivities in protein profiling experiments here provides strong evidence for this argument (Fig. 7).

In summary, we emphasize that the mass transport limitations in the kinetics of protein microspot reactions present a serious issue, which deserves further detailed studies, both theoretical and experimental. These seem to be one of the most important hurdles to be overcome for further improvement of the current microarray sensitivity and precision. The sensitivity of kinetically optimized microarrays has been improved by factors in the range of $100–10^5$ as compared with non-optimized systems. Despite the prevailing view that such simple detection approaches as applied here lack sensitivity (2, 8), we could still obtain strong signal-to-noise ratios for all anti-cytokine antibodies spotted (Fig. 7B). The applicability of the simplest and most inexpensive detection strategies for the analysis of complex clinical specimens opens additional possibilities for uncomplicated, cost-effective, highly sensitive, and unlimitedly multiplexed microspot immunoassays.

REFERENCES

1. Kusnezow, W., and Hoheisel, J. D. (2002) Antibody microarrays: promises and problems. *BioTechniques* (suppl.) 14–23
2. Haab, B. B. (2005) Antibody arrays in cancer research. *Mol. Cell. Proteomics* **4,** 377–383
3. Nielsen, U. B., and Geierstanger, B. H. (2004) Multiplexed sandwich assays in microarray format. *J. Immunol. Methods* **290,** 107–120
4. Kusnezow, W., and Hoheisel, J. D. (2003) Solid supports for microarray immunoassays. *J. Mol. Recognit.* **16,** 165–176
5. Kusnezow, W., Pulli, T., Witt, O., and Hoheisel, J. D. (2004) Solid support for protein microarrays and related devices, in *Protein Microarrays* (Schena, M., ed) pp. 247–284, Jones and Bartlett Publishers, Sudbury, MA
6. Pavlickova, P., Schneider, E. M., and Hug, H. (2004) Advances in recombinant antibody microarrays. *Clin. Chim. Acta* **343,** 17–35
7. Angenendt, P. (2005) Progress in protein and antibody microarray technology. *Drug Discov. Today* **10,** 503–511
8. MacBeath, G. (2002) Protein microarrays and proteomics. *Nat. Genet.* **32,** **(**suppl.) 526–532
9. Schweitzer, B., Roberts, S., Grimwade, B., Shao, W., Wang, M., Fu, Q., Shu, Q., Laroche, I., Zhou, Z., Tchernev, V. T., Christiansen, J., Velleca, M., and Kingsmore, S. F. (2002) Multiplexed protein profiling on microarrays by rolling-circle amplification. *Nat. Biotechnol.* **20,** 359–365
10. Saviranta, P., Okon, R., Brinker, A., Warashina, M., Eppinger, J., and Geierstanger, B. H. (2004) Evaluating sandwich immunoassays in microarray format in terms of the ambient analyte regime. *Clin. Chem.* **50,** 1907–1920
11. Sukhanov, S., and Delafontaine, P. (2005) Protein chip-based microarray profiling of oxidized low density lipoprotein-treated cells. *Proteomics* **5,** 1274–1280
12. Pawlak, M., Schick, E., Bopp, M. A., Schneider, M. J., Oroszlan, P., and Ehrat, M. (2002) Zeptosens' protein microarrays: a novel high performance microarray platform for low abundance protein analysis. *Proteomics* **2,** 383–393
13. Ekins, R. P. (1998) Ligand assays: from electrophoresis to miniaturized microarrays. *Clin. Chem.* **44,** 2015–2030
14. Ekins, R., and Chu, F. (1992) Multianalyte microspot immunoassay. The microanalytical 'compact disk' of the future. *Ann. Biol. Clin.* **50,** 337–353
15. Kusnezow, W., Syagailo, Y. V., Ruffer, S., Klenin, K., Sebald, W., Hoheisel, J. D., Gauer, C., and Goychuk, I. (2006) Kinetics of antigen binding to antibody microspots: strong limitation by mass transport to the surface. *Proteomics* **6,** 794–803
16. Kusnezow, W., Syagailo, Y. V., Goychuk, I., Hoheisel, J. D., and Wild, D. G. (2006) Antibody microarrays: the crucial impact of mass transport on assay kinetics and sensitivity. *Expert Rev. Mol. Diagn.* **6,** 111–124
17. Klenin, K. V., Kusnezow, W., and Langowski, J. (2005) Kinetics of protein binding in solid-phase immunoassays: theory. *J. Chem. Phys.* **122,** 214715
18. Goldstein, B., Coombs, D., He, X., Pineda, A. R., and Wofsy, C. (1999) The influence of transport on the kinetics of binding to surface receptors: application to cells and BIAcore. *J. Mol. Recognit.* **12,** 293–299
19. Schuck, P., and Minton, A. P. (1996) Analysis of mass transport-limited binding kinetics in evanescent wave biosensors. *Anal. Biochem.* **240,** 262–272
20. Schuck, P. (1996) Kinetics of ligand binding to receptor immobilized in a polymer matrix, as detected with an evanescent wave biosensor. I. A computer simulation of the influence of mass transport. *Biophys. J.* **70,** 1230–1249
21. Kusnezow, W., Jacob, A., Walijew, A., Diehl, F., and Hoheisel, J. D. (2003) Antibody microarrays: an evaluation of production parameters. *Proteomics* **3,** 254–264
22. Toegl, A., Kirchner, R., Gauer, C., and Wixforth, A. (2003) Enhancing results of microarray hybridizations through microagitation. *J. Biomol. Tech.* **14,** 197–204
23. Corless, R. M., Gonnet, G. H., Hare, D. E. G., Jeffrey, D. J., and Knuth, D. E. (1996) On the Lambert W function. *Adv. Comput. Math.* **5,** 329–359
24. Nygren, H., and Stenberg, M. (1989) Immunochemistry at interfaces. *Immunology* **66,** 321–327
25. Stenberg, M., and Nygren, H. (1985) A diffusion limited reaction theory for a solid-phase immunoassay. *J. Theor. Biol.* **113,** 589–597
26. Stenberg, M., and Nygren, H. (1988) Kinetics of antigen-antibody reactions at solid-liquid interfaces. *J. Immunol. Methods* **113,** 3–15
27. Berg, O. G., and von Hippel, P. H. (1985) Diffusion-controlled macromolecular interactions. *Annu. Rev. Biophys. Biophys. Chem.* **14,** 131–160
28. Zwanzig, R., and Szabo, A. (1991) Time dependent rate of diffusion-influenced ligand binding to receptors on cell surfaces. *Biophys. J.* **60,** 671–678
29. Weidemann, T., Wachsmuth, M., Knoch, T. A., Muller, G., Waldeck, W., and Langowski, J. (2003) Counting nucleosomes in living cells with a combination of fluorescence correlation spectroscopy and confocal imaging. *J. Mol. Biol.* **334,** 229–240
30. Baudendistel, N., Muller, G., Waldeck, W., Angel, P., and Langowski, J. (2005) Two-hybrid fluorescence cross-correlation spectroscopy detects protein-protein interactions in vivo. *Chemphyschem* **6,** 984–990
31. Tilton, R. D., Gast, A. P., and Robertson, C. R. (1990) Surface diffusion of interacting proteins. Effect of concentration on the lateral mobility of adsorbed bovine serum albumin. *Biophys. J.* **58,** 1321–1326
32. Zhdanov, V. P., and Kasemo, B. (2000) Monte Carlo simulation of diffusion of adsorbed proteins. *Proteins* **39,** 76–81
33. Chan, V., Graves, D. J., and McKenzie, S. E. (1995) The biophysics of DNA hybridization with immobilized oligonucleotide probes. *Biophys. J.* **69,** 2243–2255
34. Berg, O. G. (1985) Orientation constraints in diffusion-limited macromolecular association. The role of surface diffusion as a rate-enhancing mechanism. *Biophys. J.* **47,** 1–14
35. Wang, D., Gou, S. Y., and Axelrod, D. (1992) Reaction rate enhancement by surface diffusion of adsorbates. *Biophys. Chem.* **43,** 117–137
36. Axelrod, D., and Wang, M. D. (1994) Reduction-of-dimensionality kinetics at reaction-limited cell surface receptors. *Biophys. J.* **66,** 588–600
37. Erickson, D., Li, D., and Krull, U. J. (2003) Modeling of DNA hybridization kinetics for spatially resolved biochips. *Anal. Biochem.* **317,** 186–200
38. Levicky, R., and Horgan, A. (2005) Physicochemical perspectives on DNA microarray and biosensor technologies. *Trends Biotechnol.* **23,** 143–149
39. Adam, G., and Delbrück, M. (1968) Reduction of dimensionality in biological diffusion process, in *Structural Chemistry and Molecular Biology* (Rich, A., Davidson, N., eds) pp. 198–215, W. H. Freeman and Co., Publishers, San Francisco
40. Fang, F., and Szleifer, I. (2001) Kinetics and thermodynamics of protein adsorption: a generalized molecular theoretical approach. *Biophys. J.* **80,** 2568–2589
41. Read, M. J., Mayes, A. M., and Burkett, S. L. (2004) Effects of temperature and pH on the helicity of a peptide adsorbed to colloidal silica. *Colloids Surf. B Biointerfaces* **37,** 113–127
42. Doherty, E. A., Kan, C. W., and Barron, A. E. (2003) Sparsely cross-linked "nanogels" for microchannel DNA sequencing. *Electrophoresis* **24,** 4170–4180
43. Lin, F. Y., Chen, W. Y., and Hearn, M. T. (2001) Microcalorimetric studies on the interaction mechanism between proteins and hydrophobic solid surfaces in hydrophobic interaction chromatography: effects of salts, hydrophobicity of the sorbent, and structure of the protein. *Anal. Chem.* **73,** 3875–3883
44. Lin, F. Y., Chen, W. Y., and Hearn, M. T. (2002) Thermodynamic analysis of the interaction between proteins and solid surfaces: application to liquid chromatography. *J. Mol. Recognit.* **15,** 55–93
45. Jones, L. S., Peek, L. J., Power, J., Markham, A., Yazzie, B., and Middaugh, C. R. (2005) Effects of adsorption to aluminum salt adjuvants on the structure and stability of model protein antigens. *J. Biol. Chem.* **280,** 13406–13414
46. Huang, N.-P., Michel, R., Voros, J., Textor, M., Hofer, R., Rossi, A., Elbert, D. L., Hubbell, J. A., and Spencer, D. (2001) Poly(L-lysine)-*g*-poly(ethylene glycol) layers on metal oxide surfaces: surface-analytical characterization and resistance to serum and fibrinogen adsorption. *Langmuir* **17,**

489–498

47. Hlady, V. V., and Buijs, J. (1996) Protein adsorption on solid surfaces. *Curr. Opin. Biotechnol.* **7,** 72–77

48. Rossier, J. S., Gokulrangan, G., Girault, H. H., Svojanovsky, S., and Wilson, G. S. (2000) Characterization of protein adsorption and immunosorption kinetics in photoablated polymer microchannels. *Langmuir* **16,** 8489–8494

49. Tengvall, P., Lundstrom, I., and Liedberg, B. (1998) Protein adsorption studies on model organic surfaces: an ellipsometric and infrared spectroscopic approach. *Biomaterials* **19,** 407–422

50. Myszka, D. G., He, X., Dembo, M., Morton, T. A., and Goldstein, B. (1998) Extending the range of rate constants available from BIACORE: interpreting mass transport-influenced binding data. *Biophys. J.* **75,** 583–594

51. Sapsford, K. E., Liron, Z., Shubin, Y. S., and Ligler, F. S. (2001) Kinetics of antigen binding to arrays of antibodies in different sized spots. *Anal. Chem.* **73,** 5518–5524

52. Miller, J. C., Zhou, H., Kwekel, J., Cavallo, R., Burke, J., Butler, E. B., Teh, B. S., and Haab, B. B. (2003) Antibody microarray profiling of human prostate cancer sera: antibody screening and identification of potential biomarkers. *Proteomics* **3,** 56–63

53. Haab, B. B., Geierstanger, B. H., Michailidis, G., Vitzthum, F., Forrester, S., Okon, R., Saviranta, P., Brinker, A., Sorette, M., Perlee, L., Suresh, S., Drwal, G., Adkins, J. N., and Omenn, G. S. (2005) Immunoassay and antibody microarray analysis of the HUPO Plasma Proteome Project reference specimens: systematic variation between sample types and calibration of mass spectrometry data. *Proteomics* **5,** 3278–3291